1266–1279 *Nucleic Acids Research, 2018, Vol. 46, No. 3* *Published online 13 December 2017*
doi: 10.1093/nar/gkx1258

ZNF830 mediates cancer chemoresistance through promoting homologous-recombination repair

Guo Chen[1,2,*,†], Jianxiang Chen[1,3,4,†], Yiting Qiao[1], Yaru Shi[5], Wei Liu[5,6], Qi Zeng[5], Hui Xie[5], Xiaorui Shi[5], Youwei Sun[2], Xu Liu[7], Tongyu Li[1], Liqian Zhou[1], Jianqin Wan[1], Tian Xie[3], Hangxiang Wang[1,*] and Fu Wang[5,*]

[1]The First Affiliated Hospital, Collaborative Innovation Center for Diagnosis and Treatment of Infectious Diseases, Key Laboratory of Combined Multi-Organ Transplantation, Ministry of Public Health and Key Laboratory of Organ Transplantation of Zhejiang Province, School of Medicine, Zhejiang University, Hangzhou 310003, PR China, [2]Department of Radiation Oncology, Emory University School of Medicine and Winship Cancer Institute of Emory University, Atlanta, GA 30322, USA, [3]Holistic Integrative Pharmacy Institutes (HIPI), Hangzhou Normal University, Key Laboratory of Elemene Class Anti-cancer Chinese Medicine of Zhejiang Province, Engineering Laboratory of Development and Application of Traditional Chinese Medicine from Zhejiang Province, Hangzhou 311100, PR China, [4]Laboratory of Cancer Genomics, Division of Cellular and Molecular Research, Humphrey Oei Institute of Cancer Research, National Cancer Centre, Singapore 169610, Singapore, [5]Engineering Research Center of Molecular and Neuro Imaging, Ministry of Education, School of Life Science and Technology, Xidian University, Xi'an 710071, China, [6]Department of Hepatobiliary Surgery, Xijing Hospital, The Fourth Military Medical University, Xi'an, Shaanxi 710032, China and [7]Department of Biochemistry, Emory University School of Medicine, Atlanta, GA 30322, USA

Received September 14, 2017; Revised December 03, 2017; Editorial Decision December 04, 2017; Accepted December 06, 2017

ABSTRACT

Homologous recombination (HR), which mediates the repair of DNA double-strand breaks (DSB), is crucial for maintaining genomic integrity and enhancing survival in response to chemotherapy and radiotherapy in human cancers. However, the mechanisms of HR repair in treatment resistance for the improvement of cancer therapy remains unclear. Here, we report that the zinc finger protein 830 (ZNF830) promotes HR repair and the survival of cancer cells in response to DNA damage. Mechanistically, ZNF830 directly participates in DNA end resection via interacting with CtIP and regulating CtIP recruitment to DNA damage sites. Moreover, the recruitment of ZNF830 at DNA damage sites is dependent on its phosphorylation at serine 362 by ATR. ZNF830 directly and preferentially binds to double-strand DNA with its 3′ or 5′ overhang through the Zinc finger (Znf) domain, facilitating HR repair and maintaining genome stability. Thus, our study identified a novel function of ZNF830 as a HR repair regulator in DNA end resection, conferring the chemoresistance to genotoxic therapy for cancers those that overexpress ZNF830.

INTRODUCTION

DNA double-strand breaks (DSBs) are highly toxic lesions that can be generated by a variety of exogenous sources including ionizing radiation, mutagenic chemicals and chemotherapeutic drugs (1). DSBs can also arise from endogenous oxidative stress and replication fork collapse triggered by problems encountered during DNA replication (2). Failures to correctly repair DSBs may result in propagation of mutations, chromosomal translocations, genome instability, tumorigenesis, cell senescence and death (3). Therefore, it is crucial that cells must quickly detect DSBs and get them efficient repaired.

DNA DSBs are primarily repaired by two major pathways: homologous recombination (HR) and non-homologous end-joining (NHEJ) (4). NHEJ is active in all phase of cell cycle, while HR, which requires the identical sister chromatid as the template for completing the repair, occurs preferentially in S and G2 phase (4–7). NHEJ directly ligates the broken DNA ends, usually causing small deletions and additions, thus, it is considered as error-prone repair (8). Whereas HR requires sequence-homologous template to repair and restore the broken DNA molecules, therefore, HR repair is considered as error-free process (4).

NHEJ and HR repairs are executed by different machineries, respectively. NHEJ is initiated by recogni-

*To whom correspondence should be addressed. Tel: +86 571 88208152; Fax: +86 571 88208152; Email: wanghx@zju.edu.cn
Correspondence may also be addressed to Fu Wang. Tel: +86 29 81891070; Fax: +86 29 81891060; Email: fwang@xidian.edu.cn
Correspondence may also be addressed to Guo Chen. Email: guo.chen84@outlook.com
†These authors contributed equally to this work as first authors.

tion and binding of the Ku70/Ku80 heterodimer to the DNA ends, followed by the recruitment and activation of DNA-dependent protein kinase (DNA-PKcs) and the XRCC4/ligase IV complex, which joins the DNA ends together (9). During HR, DSBs is firstly recognized by MRN complex (Mre11–Rad50–NBS1) and initiated by MRN mediated DSB end resection and generating 3′ single-stranded DNA (ssDNA) overhangs (10). The resulted ssDNA overhang is rapidly bound by replication protein A (RPA), which is subsequently displaced by Rad51 recombinase (11,12). Rad51 coats on ssDNA and form a nucleoprotein filament that allows strand invasion and homology search (11). During the DNA end resection, CtIP (also known as RBBP8) is recruited to the DSBs sites and interacts with MRN (7,13). CtIP promotes end resection through stimulating the nuclease activity of MRN, accelerating generation of ssDNA regions (13). DNA end resection is the key and the rate-limiting step for HR repair, it is also considered as the determinant of the choice between HR and NHEJ (5).

Cancer cells are characterized by uncontrolled cell proliferation and division, leading to a higher chance of DNA damage including single-strand breaks (SSBs) and double-strand breaks (DSBs) during replication (14). Radiotherapy, as well as many widely used chemotherapeutic drugs, such as cisplatin, etoposide, hydroxyurea and camptothecin, are designed to induce DNA DSBs preferentially in replicating cells (15). Excessive DSBs beyond the repairing capacity would cause cell death, however, cancer cells with elevated DNA repair capacity exhibit intrinsic resistance, undermining the efficacy of such therapies (16). On the other hand, the dependence on DNA repair pathways makes them promising targets of cancer therapies. For example, a subgroup of breast cancers show defects of HR-mediated DNA repairing due to mutations of BRCA1/2, making them vulnerable to inhibitors of Poly(ADP-ribose) polymerase (PARP), a key protein involved in repairing SSBs and HR-mediated restart of stalled replication forks (17). Olaparib, the recently approved inhibitor to PARP, is now the first-in-class monotherapy for advanced ovarian cancer patients with deletion or mutation of BRCA1/2 (17–19). Clinically, the integrity of HR repair pathway has been used to predict patients' sensitivity to PARP inhibitors (17–19). Given the importance of HR repair in cancer drug response and chemoresistance, a thorough understanding of HR repair process by uncovering novel HR repair regulators would provide great therapeutic benefits.

ZNF830, also known as Ccdc16 or Omcg1, is a nuclear zinc finger protein that participates in pre-mRNA splicing (20). ZNF830 has also been implicated in DNA damage repair, since its inactivation leads to extensive DNA damage, genomic instabilities and cell death (20). In this report, we show that ZNF830 is recruited to the DSB sites through ataxia telangiectasia and rad3-related (ATR) signaling upon DNA damage, and ZNF830 directly interacts with CtIP to promote its recruitment to the sites of DSBs, thus accelerating end resection during HR repair. By regulating HR-mediated DNA repair, ZNF830 promotes cellular survival upon DNA damage and mediates the resistance of cancer cells to DNA damage caused by chemotherapies and radiotherapies.

MATERIALS AND METHODS

HR and NHEJ measurement

HR activity was measured using DR-GFP reporter system as described previously (21). Briefly, U2OS DR-GFP cells were transfected with Ctrl siRNA or ZNF830 siRNA using lipofectamine 2000™. Twenty-four hours after siRNA transfection, cells were transfected with pCBASceI plasmid to induce double strand break, followed by flow cytometry analysis for GFP recovery at 48 h latter. NHEJ was analyzed using pimEJ5GFP reporter system as described previously (22). Firstly, pimEJ5GFP plasmid was stably transfected into H1299 cells. Then, H1299 EJ5GFP cells were transfected with Ctrl siRNA or ZNF830 siRNA. 24 hrs after siRNA transfection, cells were transfected with pCBASceI. Forty eight hours after pCBASceI transfection, GFP positive cells were quantified by flow cytometry.

Immunofluorescence assay

Cells were grown on chamber slides (BD Falcon, MA, USA), fixed with 4% paraformaldehyde for 15 min, permeabilized with 0.5% Triton X-100 in PBS for 10 min and blocked with 10% normal goat serum (Life technologies, Carlsbad, CA, USA) for 1 h. Cells were then incubated with primary antibodies overnight at 4°C, after washing, samples were incubated with Alexa Fluor 488 or Alexa Fluor 555 labeled secondary antibodies for 45 min at room temperature in the dark. After washing, samples were mounted with Prolong Gold antifade reagent containing DAPI (Invitrogen). Images were captured using LSM 510 confocal microscope (Zeiss, Sweden). For RPA and CtIP foci detection, cells were pre-extracted with pre-extraction buffer (25 mM HEPES, pH 7.5, 50 mM NaCl, 1 mM EDTA, 3 mM $MgCl_2$, 300 mM sucrose, 0.5% Triton X-100 and 0.3 mg/ml RNase A) for 5 min at room temperature before being subjected to fixation.

Electrophoretic mobility shift assay (EMSA)

The DNA binding to the ZNF830 protein was determind by EMSA as described previously (23). The double-strand substrate was generated by annealing of oligonucleotide JYM698 and JYM696, the 3′-overhanging DNA duplex was produced by annealing of oligonucleotide JYM699 and JYM696 and the 5′-overhanging DNA duplex was produced by annealing of oligonucleotide JYM697 and JYM696. The sequences of oligonucleotides were: JYM696, 5′-GGG CGA ATT GGG CCC GAC GTC GCA TGC TCC TCT AGA CTC GAG GAA TTC GGT ACC CCG GGT TCG AAA TCG ATA AGC TTA CAG TCT CCA TTT AAA GGA CAA G-3′; JYM697, 5′-CTT GTC CTT TAA ATG GAG ACT GTA AGC TTA TCG ATT TCG AAC CCG GGG TA-3′; JYM698, 5′-CTT GTC CTT TAA ATG GAG ACT GTA AGC TTA TCG ATT TCG AAC CCG GGG TAC CGA ATT CCT CGA GTC TAG AGG AGC ATG CGA CGT CGG GCC CAA TTC GCC C-3′; JYM699, 5′-CCG AAT TCC TCG AGT CTA GAG GAG CAT GCG ACG TCG GGC CCA ATT CGC CC-3′. The 5′ end of JYM696 was labeled with 32P and itself without annealing was used as single-strand DNA sub-

strate. Non-labeled [γ-32P]-ATP was removed using G-25 Spin Columns. The DNA substrates were incubated with indicated ZNF830 protein in buffer (25 mM MOPS pH 7.0, 50 mM KCl, 1 mM DTT, and 1 mM $MnCl_2$) at room temperature for 15 min. DNA loading buffer (R0611, Thermo Scientific) was added to samples, subjected to 6% non-denaturing TBE (Tris–borate–EDTA)-polyacrylamide gel and analyzed by Typhoon 9210 phosphorimager (GE Healthcare).

Chromatin immunoprecipitation (ChIP) assay for measuring the DSB recruitment

U2OS-DRGFP cells, which carrying chromosomal integrated single-copy of I-SceI site, were used to detect protein recruitment to I-SceI endonuclease-induced DSB sites as described previously (24). Briefly, 24 h after transfection of indicated siRNA, cells were transfected with pCBASceI plasmids to introduce DSBs. Twenty four hours after pCBASceI transfection, ChIP assay was performed using Pierce Agarose ChIP Kit (Thermo Scientific, USA) and ZNF830 (HPA027211, Sigma) or CtIP (79809, Novus Biologicals) antibodies according to the manufacturer's instruction. The ZNF830 or CtIP associated DNA was detected by PCR using the primer at the I-SceI site. The primer sequence was: forward, 5′-TAC AGC TCC TGG GCA ACG TG-3′; reverse, 5′-TCC TGC TCC TGG GCT TCT CG-3′. The PCR program was: 95 °C for 5 min, 1 cycle; 95 °C for 45 s, 56 °C for 30 s and 72 °C for 30 s, 35 cycles; 72 °C for 10 min, 1 cycle. The amplified products were analyzed on a 1.2% agarose gel.

Xenograft tumor model

Four to six weeks of female nude mice were purchased from the animal center at The Fourth Military Medical University. All the animal protocols were performed according to the Guide for the Animal Care and Use Committee of Xidian University. For the tumor implantation, 10^7 of H1299 cells expressing control or ZNF830 shRNA were subcutaneously implanted into mouse flanks and tumors were allowed to reach 100 mm^3 before starting treatment. Mice were treated with 50 mg/kg olaparib through intraperitoneal injection (i.p.) and the vehicle group received PBS as control. Tumor volumes were measured at every 5 days and calculated by equation of $V = (L \times W^2)/2$ (V, volume; L, length; W, width) as described (25).

In vitro ATR kinase assay

In vitro analysis of ATR phosphorylates ZNF830 was performed as previously described (26). Briefly, H1299 cells were treated with 10 Gy of IR and active ATR kinase was immunoprecipitated from irradiated cells 30 min after treatment. To obtain Flag-ZNF830 WT or S362A proteins, 293T cells were transfected with Flag-ZNF830 WT or S362A mutant plasmid, and the proteins were immunoprecipitated 48 hrs after transfection. Then, the active ATR was mixed with 1 μg of purified Flag-ZNF830 proteins in 50 μl kinase buffer (10 mM HEPES pH 7.4, 50 mMNaCl, 10 mM $MgCl_2$, 10 mM $MnCl_2$, 1 mM DTT, 10 μM cold ATP and 25 μCi [γ-^{32}P] ATP) supplemented with protease inhibitor cocktail at 30°C for 1 h. Then, 2 × SDS sample buffer was added to stop the reaction, boiled and subjected to SDS-PAGE. The radiolabeled phosphorylated ZNF830 was detected using Typhoon 9210 phosphorimager (GE Healthcare).

Immunohistochemistry assay

Human lung cancer tissue microarray (HLugA150cs02) was purchased from Shanghai outdo Biotech Co., Ltd (Shanghai, China). In the microarray, 75 lung cancer tissues and their adjacent lung tissues were conducted in formalin-fixed paraffin-embedded sections. Xenograft tumors were collected and fixed in formalin, embedded in paraffin and cut into 5 μm-thick sections. Sections were firstly deparaffinized with 100% xylene, followed by rehydration using gradient ethanol (100%, 95%, 70%, 30%, 0%). After inactivation of endogenous peroxidase and retrieval antigen, IHC staining was performed using R.T.U Vectastain Kit (Vector Laboratories) according to manufacturer's instructions. The primary antibodies were ZNF830 (1:100, Sigma), Ki-67 (1:800, Abcam) and γH2AX (1:500, EMD Millipore). The percentage of Ki-67 and γH2AX positive cells was determined from three separate fields in each of three independent tumor samples. The semi-quantitation of ZNF830 staining was carried out by immunoscore (27). The immunoscore was calculated by multiplying the intensity and percentage of positive staining. The intensity was defined as follows: 0, no appreciable staining; 1, weak intensity; 2, moderate intensity; 3, strong intensity; 4, very strong intensity. High ZNF830 was defined when immunoscore $\geq$ 100; Low ZNF830 was defined when immunoscore $<$ 100.

Metaphase spread assay

H1299 cells were transfected control or ZNF830 siRNA, and then treated with 5 Gy of IR. Twelve hours after IR treatment, cells were exposed to 1 μg/ml colcemid (Thermo Fisher Scientific, Somerset, NJ) for 1.5 h and cells were then suspended in 0.56% KCl 15 min at 37°C. After fixing in methanol/acetic acid (3:1) (vol/vol) for 20 min in –20°C, cells were dropped onto slides and air dried. After mounted with DAPI, the spreads were detected under fluorescence microscopy.

Statistical analysis

The statistical significance of differences between groups was analyzed with two-sided unpaired student's t-test or Fisher's exact test. Results were considered statistically significant at $P < 0.05$. All data are presented as mean ± standard deviation (S.D.).

RESULTS

ZNF830 enhances cell survival in response to DNA damage agents

ZNF830 was predicted as an essential gene for the sustained growth of cancers in whole genome-scale CRISPR

screen (28), but its biological functions are still unknown. To analyze the role of ZNF830 in cancer progression, we utilized the Kaplan–Meier plotter on-line database (http://kmplot.com/analysis/) and found that high expression of ZNF830 is associated with poor survival in lung and gastric cancer patients (Figure 1A). Moreover, we evaluated ZNF830 protein levels in adjacent normal lung tissues and lung tumors, immunochemistry (IHC) assay showed that ZNF830 protein levels were elevated in lung tumors (Figure 1B). Meanwhile, knocking down of ZNF830 by shRNA attenuated the growth of H1229 and A549, two human lung cancer cell lines (Supplementary Figure S1A). Given that ZNF830 is a nuclear protein and harbors zinc finger (ZNF) DNA binding motif (20), we next tested whether ZNF830 is involved in the regulation of cancer cell survival in response to DNA damage agents. The clonogenic survival assay revealed that the knockdown of ZNF830 sensitized H1299 cells to ionizing radiation (IR), hydroxyurea (Hu) and camptothecin (CPT) (Figure 1C). To confirm the pro-survival role of ZNF830 to DNA damage agents, we employed CRISPR-Cas9 to deplete ZNF830 in A549 cells and we obtained similar results in ZNF830-depleted A549 cells treated with IR, Hu and CPT (Supplementary Figure S1B).

ZNF830 regulates HR repair

We then examined γH2AX level, which is the ser139 phosphorylation of H2AX and recognized as marker of DNA damage (29), after IR treatment. We detected a significant increase of γH2AX at 0.2 h, which was gradually reduced to the initial level at 24 h after IR in the control siRNA transfected H1299 cells or A549 parental cells, but we found a delayed clearance of γH2AX in ZNF830 silenced-cells or ZNF830 knock out cells (Figure 2A and Supplementary Figure S2A). These data suggest that ZNF830 may be involved in regulation of DNA damage response (DDR) or/and possibly the repair of DNA damage. Since activation of Chk1 and Chk2 are the major effectors for DNA damage response signaling (30), we thus examined Chk1 and Chk2 phosphorylation after IR treatment, and we detected a similar pattern of Chk1 and Chk2 phosphorylation in H1299 cells treated with control siRNA or siRNA against ZNF830 (Supplementary Figure S2B). This result indicates ZNF830 may not directly affect DDR signaling.

DNA DSBs are mainly repaired by HR and NHEJ repair pathways (4). We next employed reporter systems to measure the HR and NHEJ activity. In HR reporter substrate (pDR-GFP), the GFP gene is interrupted by I-SceI site and the functional GFP can only be restored by HR repair using the downstream iGFP sequence as the template after I-SceI expression (Figure 2B) (21). Using U2OS DR-GFP cells, which harboring chromosomally integrated single-copy of the DR-GFP construct (31), the percentage of GFP-positive cells was significantly reduced in cells treated with siRNA against ZNF830 after exogenous expression of I-SceI, indicating a suppression of HR repair pathway after ZNF830 knock-down (Figure 2C). In addition, we also employed NHEJ reporter (EJ5-GFP), in which the puro gene is inserted into a I-SceI site between the promoter and the open reading frame of GFP, and the GFP can only be expressed via NHEJ repair pathway after the removal of puro gene by exogenously expressed I-SceI (Figure 2B) (22). Different from the result of HR reporter assay, no significant change of GFP-positive rates was detected after the silencing of ZNF830 in H1299 cells with stably transfected EJ5-GFP plasmid (Figure 2D). Meanwhile, we did not detect significant change in cell cycle progression after knockdown of ZNF830 (Supplementary Figure S2C). These results suggest that ZNF830 mainly affects HR, but not NHEJ repair pathway after DNA damage.

Loading of Rad51 onto the resected single-strand DNA (ssDNA) is the critical step during HR process and Rad51 foci formation is considered as the marker of HR repair (11). To confirm the role of ZNF830 in HR repair pathway, Rad51 foci were stained in H1299 cells after IR treatment. In consistence with the result of previous HR reporter assay, ZNF830-silenced cells exhibited a significantly lower level of Rad51 foci formation, compared with control cells (86.1 ± 4.8% versus 35.9 ± 6.7%) (Figure 2E). At the same time, there was no significant change in the formation of 53BP1 foci, a common indicator of activated NHEJ repair pathway or DNA damage sites which have not yet been committed to repair process (6), in H1299 cells treated with siRNA against ZNF830 after the exposure to IR (Supplementary Figure S2D). Thus, our results indicated a potential role of ZNF830 in regulating of HR repair. Furthermore, we observed that ZNF830 depletion significantly increased the IR-induced chromosome aberration including chromosome and chromatid breaks by metaphase spread assay (Figure 2F). Thus, our results showed that ZNF830 has an important role in the process of HR repair.

Phosphorylation of ZNF830 at Ser362 by ATR induces its recruitment to DNA damage sites

Next, we tested whether ZNF830 could localize at the DNA damage site to support HR repair. The immunofluorescence assay showed that ZNF830 formed foci co-localized with γH2AX, the marker of DNA damage, after IR treatment (Figure 3A). To further confirm ZNF830 recruitment at DNA damage site, chromatin immunoprecipitation (ChIP) assay was employed to examine the existence of DSB fragments in the ZNF830 immunoprecipitation complex in U2OS-DRGFP cells. A clear band of DSB fragment was detected in the product of ZNF830 ChIP after the introduction of DSBs by the exogenous expression of I-SceI, but not in the product of IgGChIP (Figure 3B). Meanwhile, no DSB fragment was detected after the depletion of ZNF830 by siRNA (Figure 3B). These results indicated that ZNF830 localizes to DNA DSB sites after the induction of DNA damage.

Sensing DNA damage are orchestrated by three serine/threonine kinases named ATR, ATM and DNA-PKcs, which phosphorylate their substrates containing conserved S/TQ motif (32). So, an antibody against pS/TQ was utilized to test whether ZNF830 could be directly phosphorylated at S/TQ motif after DNA damage. We found that ZNF830 was phosphorylated at S/TQ site in response to IR, Hu or CPT treatment (Figure 3C). Two SQ motifs including S89 and S362 are in the human ZNF830 protein and we thus generated S89A or S362A substitution mutant, in which serine is replaced with alanine, to block

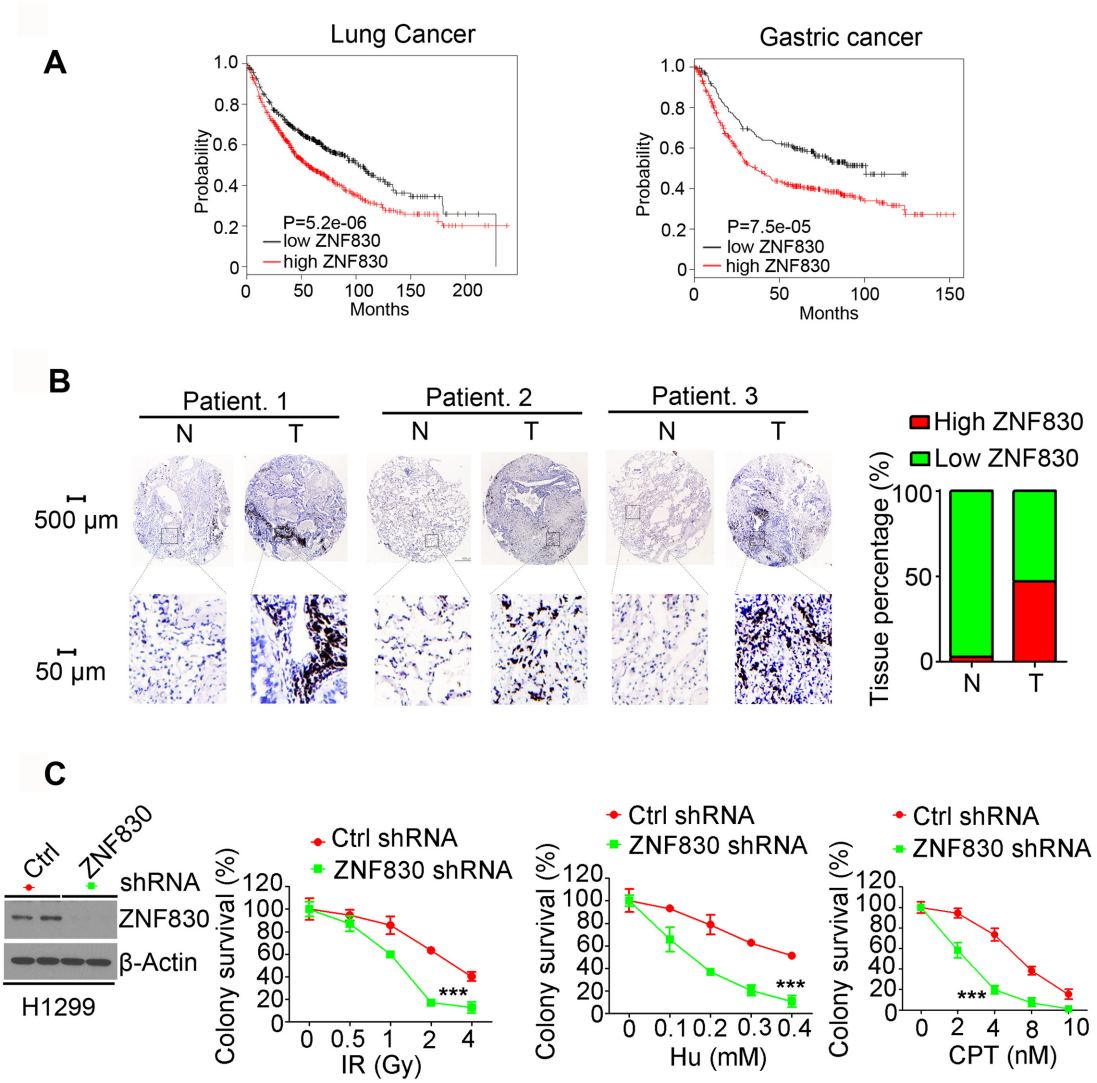

Figure 1. Depletion of ZNF830 sensitizes cancer cells to ionizing radiation (IR), hydroxyurea (Hu) and camptothecin (CPT). (**A**) Kaplan-Meier plots of lung cancer and gastric cancer patients with different ZNF830 mRNA expression (high versus low) in the KM-Plotter database (www.kmplot.com). (Affy id/Gene symbol: 226315_at; Split patients by median level; Follow up threshold: all; and auto select best cutoff were selected to generate these figures). Log-rank test *P*-value is displayed. (**B**) ZNF830 IHC staining in lung tumor tissues (T) and paired normal lung tissues (N). ZNF830 levels were quantified as described in 'Method'. $n = 75$. (**C**) H1299 cells expressing control (Ctrl) or ZNF830 shRNA were treated with indicated concentrations of IR, Hu or CPT and cultured for 10 days. The surviving colonies were counted and the relative colony survivals were normalized to untreated group. Western blot show the ZNF830 protein levels in cells expressing Ctrl or ZNF830 shRNA. ** < 0.01; *** $P < 0.001$. Data presented as mean ± SD of three independent replicates.

its phosphorylation. Intriguingly, S362A, but not S89A mutant, abolished ZNF830 phosphorylation in response to IR treatment (Figure 3D), suggesting that ZNF830 is phosphorylated at S362 site after DNA damage. Moreover, this S/TQ motif is conserved across species (Figure 3E). Next, their inhibitors against ATM, ATR or DNA-PKcs were employed to pinpoint the specific kinase mediating phosphorylation of ZNF830. Only the treatment of ATR inhibitor (VE821) abolished ZNF830 phosphorylation, while the treatment of ATM inhibitor (KU55933) or DNA-PKcs inhibitor (NU7441) exhibited no significant effect on IR-induced phosphorylation of ZNF830 (Supplementary Figure S3A), suggesting that the DNA damage-induced phosphorylation of ZNF830 is mediated by ATR. Furthermore, the *in vitro* ATR kinase assay confirmed that ATR directly phosphorylated wild-type (WT) ZNF830, but not the S362A mutant (Figure 3F). These results showed that ZNF830 was phosphorylated by ATR at S362 in response to DNA damage.

To investigate whether ZNF830 recruitment to DSB site depends on its phosphorylation, ZNF830/DSBs association was analyzed after the depletion of endogenous ATR by siRNA. The ChIP assay showed that the binding between ZNF830 and DSBs were significantly reduced in ATR-depleted cells (Supplementary Figure S3B and C), suggesting that the localization of ZNF830 at DSB sites is dependent on the ATR. Additionally, the immunofluorescence assay showed that wild-type ZNF830 formed foci

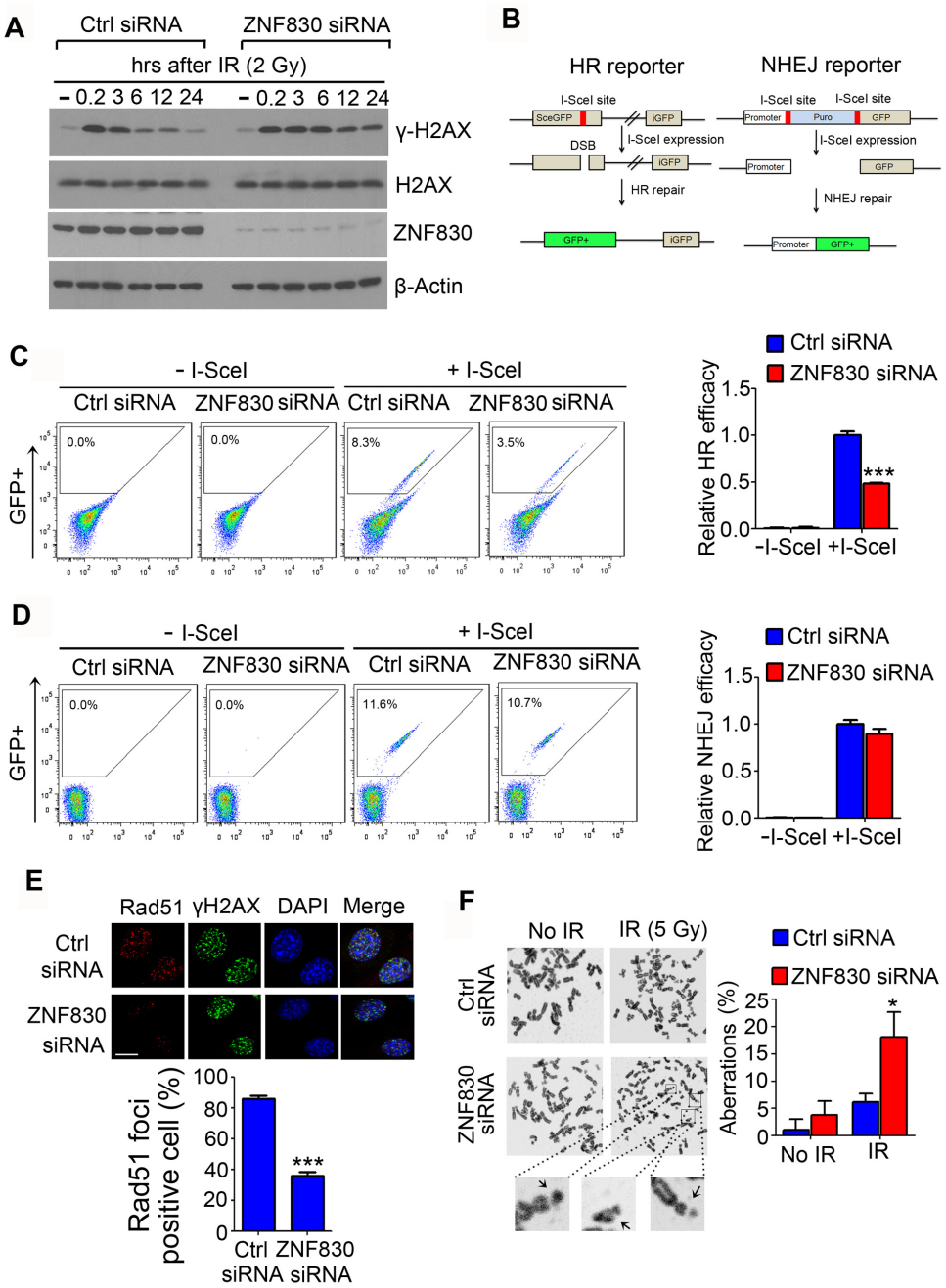

Figure 2. ZNF830 depletion impairs HR repair activity. (**A**) Knockdown of ZNF830delays γH2AX disappearance after IR. H1299 cells were treated with 2 Gy of IR and recovered for the indicated time points. γH2AX levels were examined by western blot. (**B**) Schematic diagram of HR and NHEJ reporter. (**C**) ZNF830 knockdown reduced HR repair efficacy. U2OS-DRGFP cells were transfected with control (ctrl) or ZNF830 siRNA, followed by the transfection of pCBASceI 24 h later. The GFP positive cells were recorded by flow cytometry at 48 hrs after pCBASceI transfection. Left, representative profiles were shown; Right, the relative HR repair efficacy was quantified. (**D**) Effect of ZNF830-knock down on NHEJ activity. H1299-EJ5GFP cells were transfected with Ctrl or ZNF830 siRNA, followed by pCBA-SceI transfection 24 h later and the NHEJ was measured as the percentage of GFP expressing cells by flow cytometry. Left, representative profiles were shown; Right, the relative HR repair efficacy was quantified. (**E**) Ctrl or ZNF830 siRNA transfected H1299 cells were exposed to 2 Gy of IR, cells were then stained with γH2AX and Rad51. Left, representative image; Right, quantification of mean Rad51 foci per cell. (**F**) H1299 cells transfected with control (ctrl) or ZNF830 siRNA, cells were then treated with or without 5 Gy of IR. Twelve hours after IR treatment, chromosomal aberrations were evaluated by metaphase spread assay. Data were presented as mean ± SD. $^{*}P < 0.05$, $^{***}P < 0.001$.

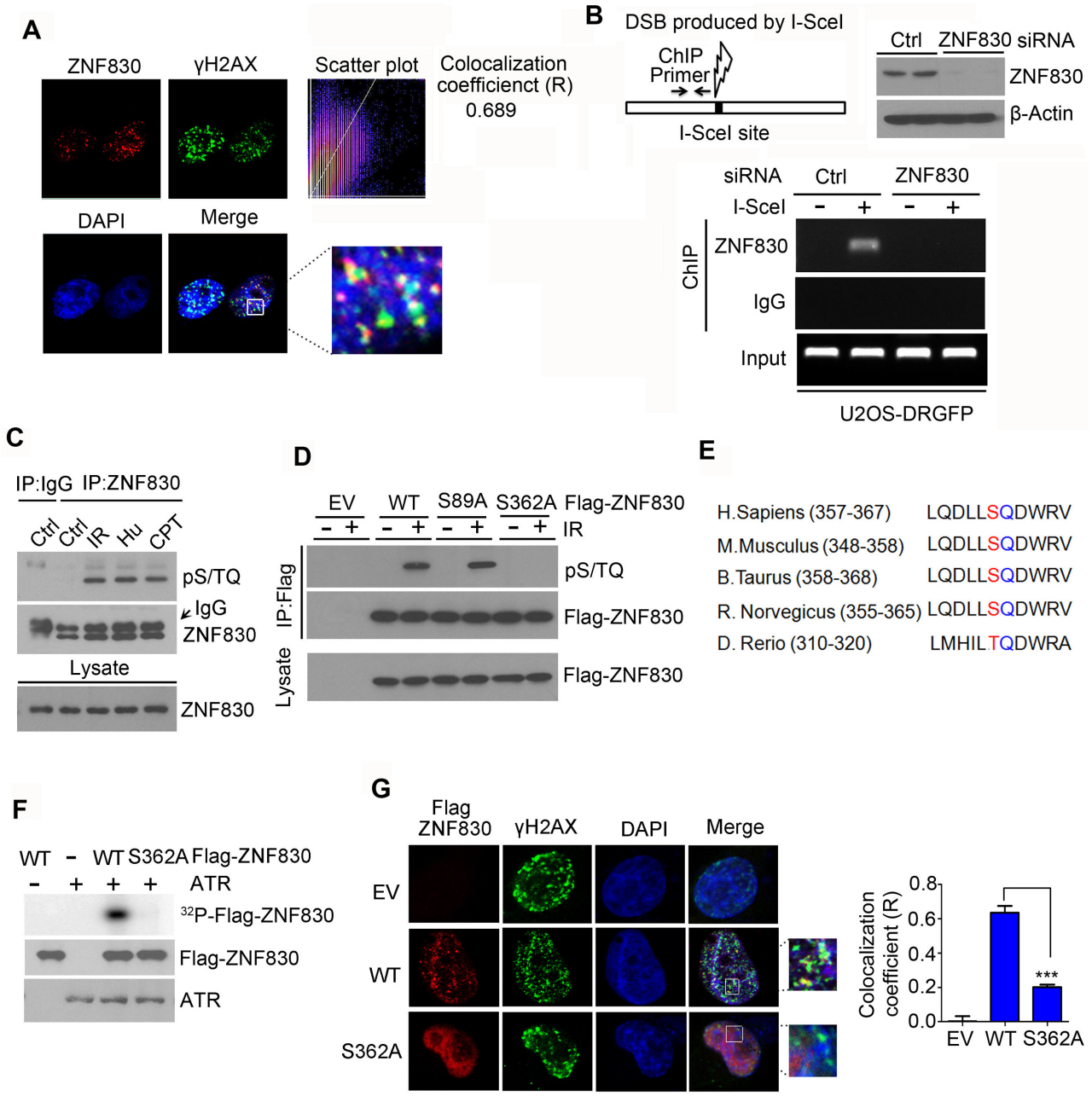

Figure 3. Recruitment of ZNF830 to the DSBs sites depends on ATR phosphorylates its Ser 362. (**A**) ZNF830 co-localizes with γH2AX upon IR treatment. H1299 cells were exposed to IR (2 Gy) and immunostained with ZNF830 and γH2AX. (**B**) U2OS DR-GFP cells were transfected with control (ctrl) or ZNF830 siRNA, 24 hrs later transfected with pCBASceI to introduce DSB, and ChIP assay was performed using anti-ZNF830 antibody, followed by PCR to detect ZNF830/DSB association. Upper right, the diagram of ChIP principle to detect ZNF830 recruitment to DSB, which was induced by I-SceI. The PCR primer locates at 100 bp upstream of DSB site. Upper left, ZNF830 depletion was confirmed by western blot; Bottom, PCR amplification of DSB fragments in the ChIP assay. (**C**) IR, Hu or CPT treatment induces ZNF830 phosphorylation. H1299 cells were treated IR (10Gy), Hu (2 mM) or CPT (1μM), followed by IP with ZNF830 and western blot analysis of ZNF830 phosphorylation using anti-phospho-ATM/ATR/DNA-PK substrate antibody. (**D**) H1299 cells were transfected with indicated Flag-ZNF830 substitution mutants, and treated with or without IR (10 Gy). Flag IP were performed and ZNF830 phosphorylation was analyzed with anti-phospho-ATM/ATR/DNA-PK substrate antibody. (**E**) Sequence alignment of conserved DNA damage induced phosphorylation motif SQ or TQ in ZNF830 across various species. (**F**) *In vitro* ATR kinase assay using purified WT or S362A Flag-ZNF830 as the substrates. (**G**) H1299 cells were transfected with WT or S362A Flag-ZNF830 mutant, and treated with IR (5 Gy) 24 h later. Co-staining of Flag and γH2AX were shown.

co-localized with γH2AX foci after IR treatment, while the S362A phosphorylation-deficient mutant failed to form such foci (Figure 3G). Thus, these results proved that ATR phosphorylates ZNF830 at S362 in response to DNA damage, resulting in the recruitment of ZNF830 to the sites of DNA damage.

ZNF830 directly and preferentially binds to dsDNA with 3′ or 5′ overhang

Since ZNF830 containing ZNF DNA binding domain (20), we then purified His tagged recombinant WT or ZNF domain deletion (ΔZNF) proteins from *E. coli* to test whether ZNF830 directly binds to double-strand DNA (dsDNA) end (Figure 4A). Both blunt and single-strand overhang ends can be generated during double-strand DNA break (33,34), so three kinds of dsDNA substrates (blunt dsDNA, 3′-overhang dsDNAor 5′-overhang dsDNA) were incubated with an increasing concentrations of WT ZNF protein or ZNF-deletion mutant and the mixture was subject to electrophoretic mobility shift assay (EMSA). Only a slight binding of blunt dsDNA was detected with 40 nM of WT ZNF830 protein (Figure 4B). Whereas, 3′ or 5′ overhang dsDNA started to show obvious binding from 10 nM WT protein, which further increased to the saturation level in the presence of higher concentrations of WT ZNF830 protein (Figure 4C and D). Meanwhile, single-strand DNA (ssDNA) could also bind to WT ZNF830 protein starting from 10 nM (Supplementary Figure S4). However, no binding of DNA substrates was detected with ΔZNF mutant protein (Figure 4B–D). These results indicated that ZNF830 protein directly binds to dsDNA through its ZNF domain, with a higher affinity to 3′ or 5′ overhang dsDNA compared to blunt dsDNA.

ZNF830 interacts with CtIP through its coiled coil domain

To test whether ZNF830 is associated with HR proteins, we performed the immunoprecipitation (IP) assay using anti-ZNF830 antibody and the results showed that ZNF830 interacts with CtIP. But we failed to observe any interaction between ZNF830 and other HR machinery components including Mre11, Rad50, NBS1, Rad51 and RPA2 (Figure 5A). The reciprocal Co-IP by the antibody against CtIP confirmed the interaction between ZNF830 and CtIP (Figure 5B). In addition, *in vitro* IP assay using recombinant His-ZNF830 and GST-CtIP proteins further confirmed that ZNF830 directly interacts with CtIP (Figure 5C).

The full length ZNF830 contains three functional domains named ZNF domain, Glu-rich domain and coiled-coil domain respectively (Figure 5D) (20). To map the CtIP-binding site of ZNF830, we generated a serial of deletion mutants of ZNP830, including ZNF deletion mutant (ΔZNF), Glu-rich domain-deletion mutant (ΔGlu) and coiled-coil domain-deletion mutant (ΔCC) (Figure 5D). The IP assay revealed that ΔCC mutant completely lost the interaction with HA-CtIP (Figure 5E), indicating that the coiled-coil domain is required for ZNF830's interaction with CtIP. Whereas, we detected similar ZNF830 foci formation and co-localization with γH2AX (Supplementary Figure S5A), implying that ZNF830 foci formation does not depends on binding to CtIP.

To study whether DNA damage affects the association between ZNF830 and CtIP, we next co-transfected H1299 cells with Flag-ZNF830 and HA-CtIP, followed by IP at 1 h after 5Gy of IR treatment, the time at which IR did not change cell cycle progression (Supplementary Figure S5B). We detected a similar level of CtIP/ZNF830 association in IR-treated cells and untreated cells (Figure 5F). Since HR repair activity is regulated by cell cycle, mainly occurring during S and G2 phase (35), the CtIP-ZNF830 association was analyzed in cells that were synchronized with double-thymidine blocking (Supplementary Figure S5C). Intriguingly, we found that CtIP-ZNF830 association was stronger during S and G2 phase, comparing with cells at G1 phase (Figure 5G). CtIP is known to be phosphorylated at Ser327 during S and G2 phase (7). Thus, S327D (phosphorylation mimics) or S327A (phosphorylation deficient) mutants of HA-CtIP were utilized to study whether this S-G2 specific phosphorylation of CtIP affects ZNF830/CtIP association. As expected, significantly more CtIP S327D mutant bound to ZNF830, compared to wild-type CtIP and S327A CtIP mutant (Figure 5H). Since phosphorylation at S327 is critical for CtIP/BRCA1 association, we then tested whether overexpression of BRCA1 could reduce CtIP interacting with ZNF830, and we detected a less level of CtIP bound to ZNF830 in presence of BRCA1 (Supplementary Figure S5D). Taking together, these results suggest that S327 phosphorylation of CtIP enhances its interaction with ZNF830during S and G2 phase.

ZNF830 promotes DNA end resection

Since ZNF830 associates with DNA damage sites (Figure 3A and B), we then tested whether ZNF830/CtIP association promotes CtIP function. The ChIP assay showed that CtIP-associated DSB fragment is significantly reduced in ZNF830 silent cells after DSB induction by I-SceI (Figure 6A). In consistence with the results of ChIP assay, the numbers of CtIP foci also decreased in ZNF830-silenced cells (Figure 6B). Moreover, WT ZNF830, but not ΔCC mutant without CtIP binding site (Figure 5E), could rescue the reduction of CtIP foci formation caused by loss of ZNF830 (Supplementary Figure S6A). These results suggest that ZNF830 promotes recruitment of CtIP at DSBs.

Since CtIP is crucial for efficient DNA end resection, we then evaluated the effect of ZNF830 depletion on DNA end resection through monitoring the RPA2 foci (13). As expected, silencing of ZNF830 led to a significant decrease of RPA2 foci level after IR treatment (Figure 6C). Similarly, re-introduction of WT ZNF830 restored RPA2 foci level in ZNF830 knock out cells, while ΔCC mutant failed to restore RPA2 foci level (Supplementary Figure S6B). RPA2 phosphorylation of Ser4/8 is considered as the marker of DNA end resection (36). We observed a robust activation of S4/S8 RPA2 phosphorylation at 60–180 min in cells treated with control siRNA, but this RPA2 S4/S8 phosphorylation were bleak in ZNF830 silenced cells (Figure 6D). These results indicate that ZNF830 is required for efficient CtIP recruitment and DNA end resection.

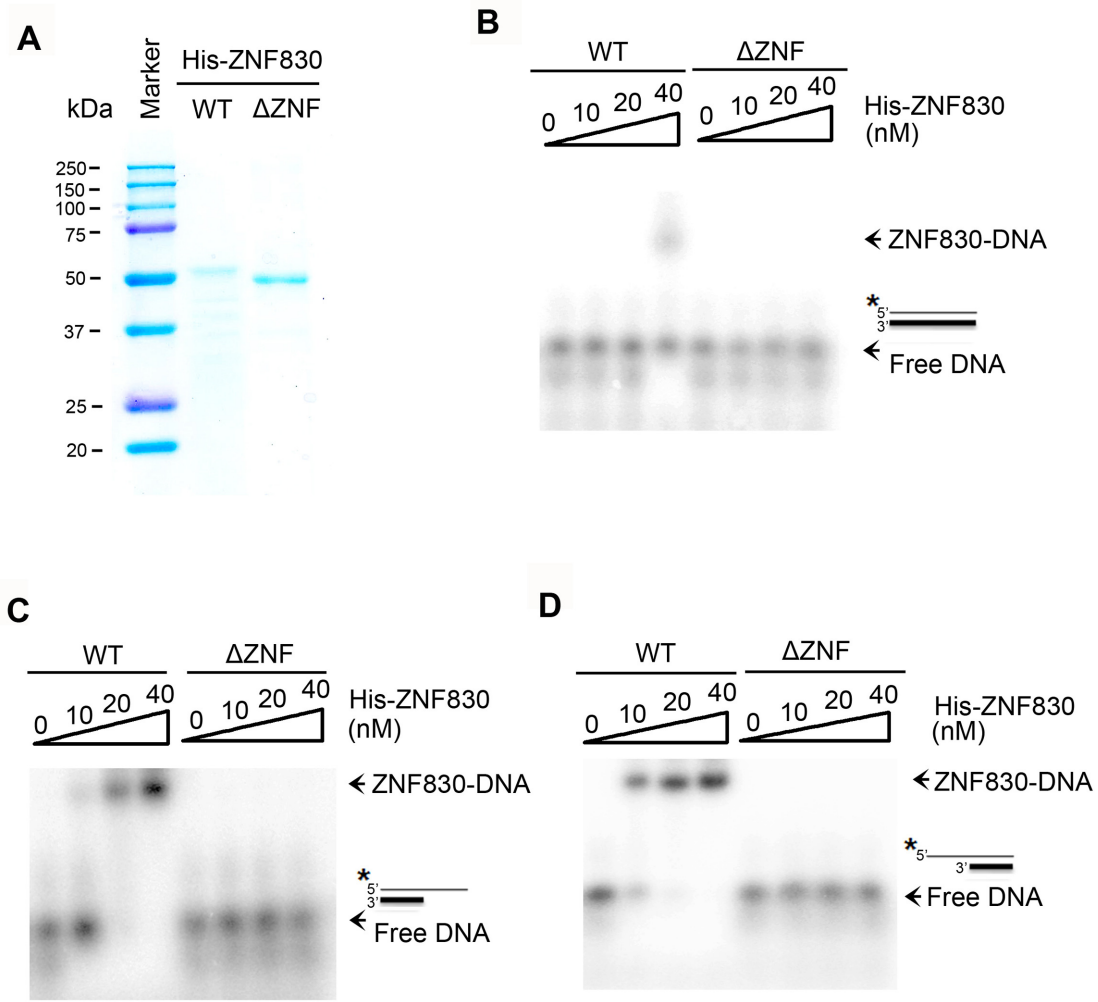

Figure 4. Purification and DNA binding activity of ZNF830. (**A**) His tagged ZNF830 WT and ΔZNF proteins were expressed and purified from *E.coli*, the proteins were analysis by 10% SDS-PAGE gel electrophoresis. (B–D) 5′-end labeled blunt double-strand DNA (dsDNA) (**B**), 3′-overhang dsDNA (**C**) or 5′-overhang dsDNA (**D**) was incubated with indicated doses of purified WT or ΔZNF His-ZNF830 protein, its DNA binding activity was analyzed by EMSA. Arrows show the free DNA and the DNA–ZNF830 complex.

Depletion of ZNF830 sensitizes lung cancer to PARP inhibitor treatment

HR repair confers resistance to DNA damage agents, especially to PARP-inhibitor therapy (16). Olaparib, a first-in-class PARP inhibitor, selectively kills HR-deficient cancer cells (18). As a HR repair regulator, we thus tested whether depletion of ZNF830 could sensitize HR-proficient lung cancer cells to olaparib treatment. As expected, the clonogenic survival assay showed that ZNF830-knockdown H1299 cells or A549 cells are more sensitive to olaparib treatment (Figure 7A). Then, we further tested the therapeutic efficacy of olaparib in H1299 lung tumor xenografts expressing control or ZNF830 shRNA. In consistence with *in vitro* clonogenic assay, we found olaparib greatly inhibited growth of ZNF830 knockdown tumors, but not in control tumors (Figure 7B and C). In addition, olaparib treatment induced more γH2AX and less Ki67 in ZNF830-knockdown xenografts (Figure 7D). These results indicate that silencing of ZNF830 sensitizes lung cancers to olaparib treatment due to impaired HR repair activity and unrepairable DNA damage.

DISCUSSION

HR-mediated DNA DSB repair is crucial for maintaining genomic integrity and survival in response to various genotoxic agents (37,38). The data presented above introduce ZNF830 as an essential component of the efficient HR repair machinery. In line with this conclusion, we showed that the depletion of ZNF830 resulted in a significant reduction of HR repair activity and survival of cells exposed to IR, hydroxyurea, CPT and olaparib. Moreover, we demonstrated that ZNF830 is a substrate of ATR, one of the major controllers of DNA damage response. ATR directly phosphorylates ZNF830 at its S362 upon DNA damage, directing its recruitment to DSB sites. Phosphorylation-resistant mutant of ZNF830 (S362A) failed to localize to the sites of DNA damage, indicating the importance of ATR-dependent recruitment of ZNF830 for its function in HR repair (Figure 3G). At the sites of DSBs, ZNF830 directly cooperates with

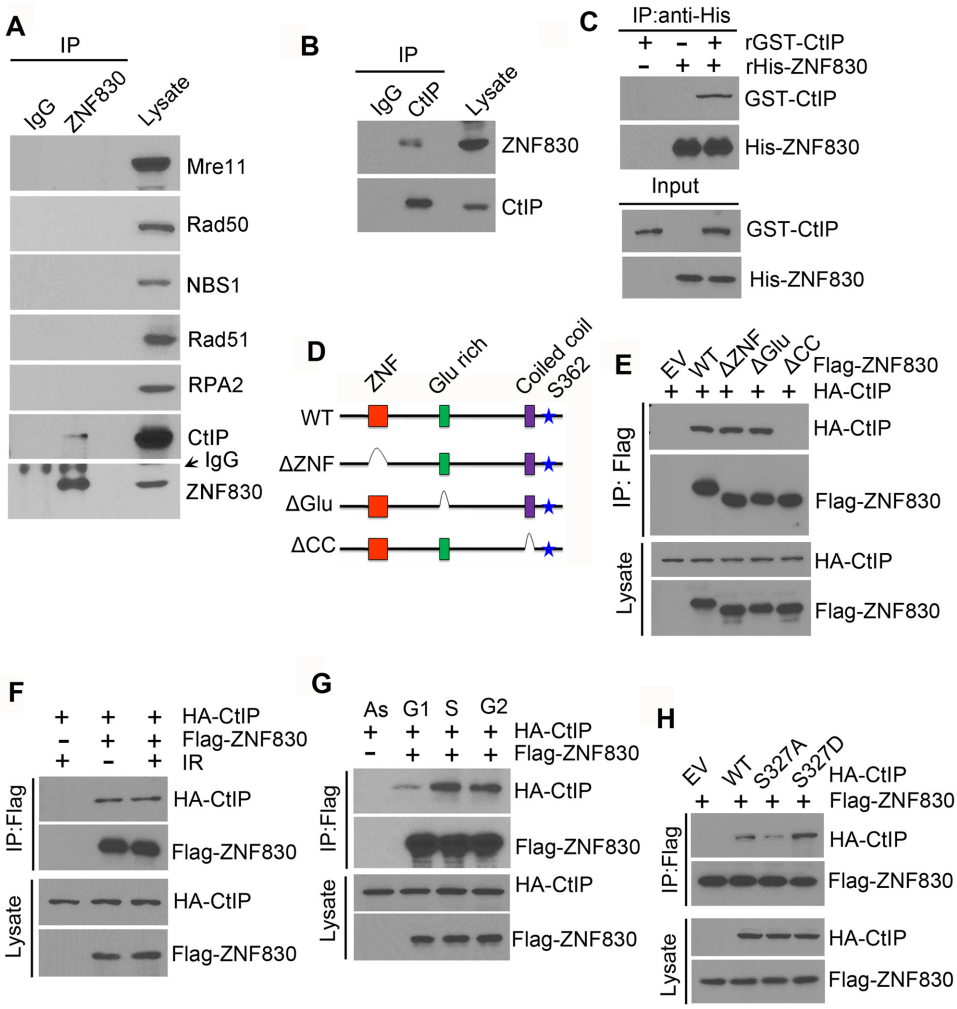

Figure 5. ZNF830 directly interacts with CtIP through its coiled-coil domain. (**A**) H1299 cells were lysed and IP was performed using anti-ZNF830 antibody and western blot with indicated HR proteins. (**B**) Endogenous interaction between ZNF830 and CtIP was confirmed by IP assay using anti-CtIP antibody and western blot assay using anti-ZNF830 or anti-CtIP antibody. (**C**) *In vitro* immunoprecipitation assay was performed using recombinant His-ZNF830 and GST-CtIP and anti-His antibody. (**D**) Schematic diagram of various ZNF830 deletion mutants. (**E**) H1299 cells were co-transfected with indicated Flag-ZNF830 variants and HA-CtIP, followed by IP with Flag and ZNF830 associated HA-CtIP was analyzed by western blot. (**F**) H1299 cells were co-transfected with HA-CtIP and Flag-ZNF830, and treated with or without 5 Gy of IR. The association between ZNF830 and CtIP was analyzed by IP with Flag at 1 hr after IR and western blot analysis with indicated antibodies. (**G**) H1299 cells were co-transfected with indicated combination of HA-CtIP and Flag-ZNF830 and synchronized at G1, S or G2 phase of cell cycle by double-thymidine block as described in "Method". IP with anti-Flag and Flag-ZNF830 associated HA-CtIP was examined by western blot. (**H**) H1299 cells were co-transfected with indicated HA-CtIP mutants and Flag-ZNF830, followed by IP with Flag and western blot with indicated antibodies.

CtIP to promote DNA end resection, therefore accelerating HR repair. On the other hand, it is known that robust ATR signaling depends on resected single-strand DNA and also supports HR repair pathway (39,40), thus, ZNF830 might not participate in the initial step of DNA end resection. ZNF830 and ATR mutually affect each other through positive feedback loop in promoting HR repair. In agreement with our observations, it has been reported that oocyte-specific knock-out of ZNF830 in mice leads to the accumulation of DNA DSBs and subsequent c-Abl/TAp63-dependent death of oocyte, mimicking premature ovarian insufficiency (POI) associated with endocrine-related disorders in 1% of women (20). Moreover, single nucleotide polymorphism of a nucleotide (rs3744355) within the single exon of the ZNF830 gene is found to be associated with the acute adverse skin reactions following radiotherapy for breast cancer (41), which might be explained by its involvement in the repair of DSBs. ZNF830 was identified as an important gene for cancers (28), our data showed that elevated ZNF830 expressions were detected more often in lung cancers compared with normal lung tissues, the specific function of ZNF830 in cancer progression still requires further investigation.

In the present study, we uncovered the role of ZNF830 in homologous recombination-mediated DNA repair and reported that ZNF830 directly interacts with CtIP, which plays critical role in promoting MRN mediated DNA end resection (7). ATR phosphorylates ZNF830 at S362 upon DNA-double strand break, which then enhances CtIP DSB recruitment, DNA end resection and HR repair (Supple-

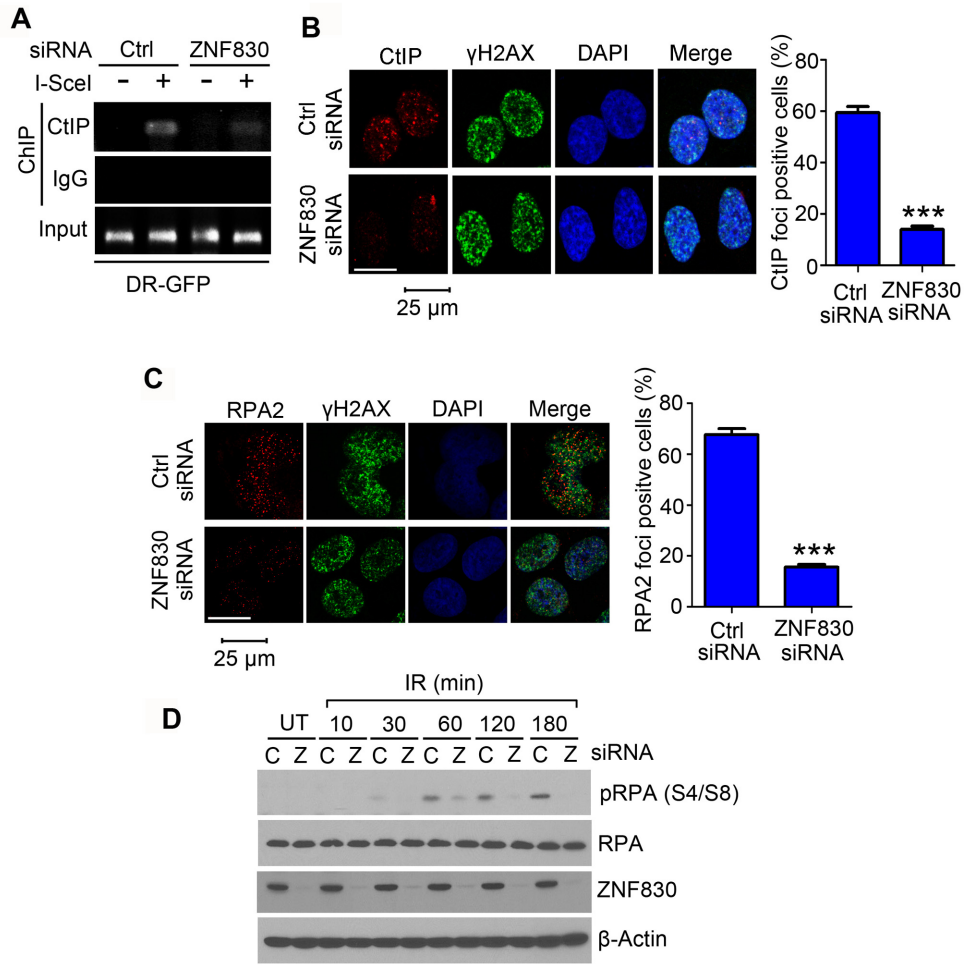

Figure 6. ZNF830 is required for efficient end resection. (**A**) U2OS-DRGFP cells were transfected ctrl or ZNF830 siRNA, followed by transfection with pCBASceI 24 h later, and ChIP assay was performed using anti-CtIP antibody, followed by PCR to detect CtIP bound DSB fragment. (B and C) H1299 cells were transfected with ctrl or ZNF830 siRNA, and treated with 10 Gy of IR. Co-staining of CtIP and γH2AX (**B**) or RPA2 andγH2AX (**C**) was performed. Left, representative image of staining were shown; Right, quantification of CtIP positive cells. (**D**) H1299 cells were transfected with control (C) or ZNF830 (Z) siRNA, and 2 days later treated with IR (10 Gy). Then, western blot assay of indicated protein levels at indicated time points recovered from IR treatment. ***$P < 0.001$. Quantitative data presented as mean ± SD of three independent replicates.

mentary Figure S6C). Due to its critical roles in DNA end resection (13), CtIP is under the coordination of many other proteins including BRCA1, And-1 and USP4 (7,42,43). The binding between BRCA1 and CtIP depends on BRCA1's phosphoylation at serine 327 in S and G2 phase during which the active HR occurs (7). And-1 constitutively interacts with CtIP, which could be enhanced by DNA damage (42). USP4 interacts with CtIP and regulates the recruitment of CtIP to DNA damage sites through its deubiquitylating enzyme activity (43). Herein, we identified ZNF830 as a new regulator of CtIP, which directly and preferentially binds to overhanging DNA ends which is preferred by HR repair pathway (13), facilitating CtIP's recruitment to the sites of DSBs by direct protein-protein interaction through its coiled-coil domain. Similar to the interaction between BRCA1 and CtIP, the association of ZNF830 and CtIP is also regulated by cell cycle progression, peaking at S and G2 phase during which HR repair is active.

ZNF830 was previously identified to interact with the XAB2 splicing complex, which also containing hAquarius, XAB2, hPRP19, hISY1, and PPIE (44). The function of XAB2 complex is involved in pre-mRNA splicing, transcription, and transcription-coupled repair (44). The depletion of XAB2 resulted in the hypersensitivity to killing by UV light in Hela cells, which could be partially explained by a decrease in recovery of RNA synthesis after UV irradiation as well as the suppression of total RNA synthesis (44). Meanwhile, a recent study reported that XAB2, which localizes adjacent to the DNA damage sites, also promotes HR repair by enhancing CtIP hyperphosphorylation and histone acetylation, whose detailed mechanism remained to be elucidated (45). Similarly, as a component of XAB2 complex, our work found that ZNF830 also participates in DSB repair via HR and plays a positive role in DNA end resection. Distinct with XAB2, our data suggested that ZNF830 promotes HR repair through directly cooperates with CtIP and enhances recruitment of CtIP to the DSB sites. Thus, our work identified a novel function of ZNF830 in DNA end resection and chemotherapeutic drug sensitivities.

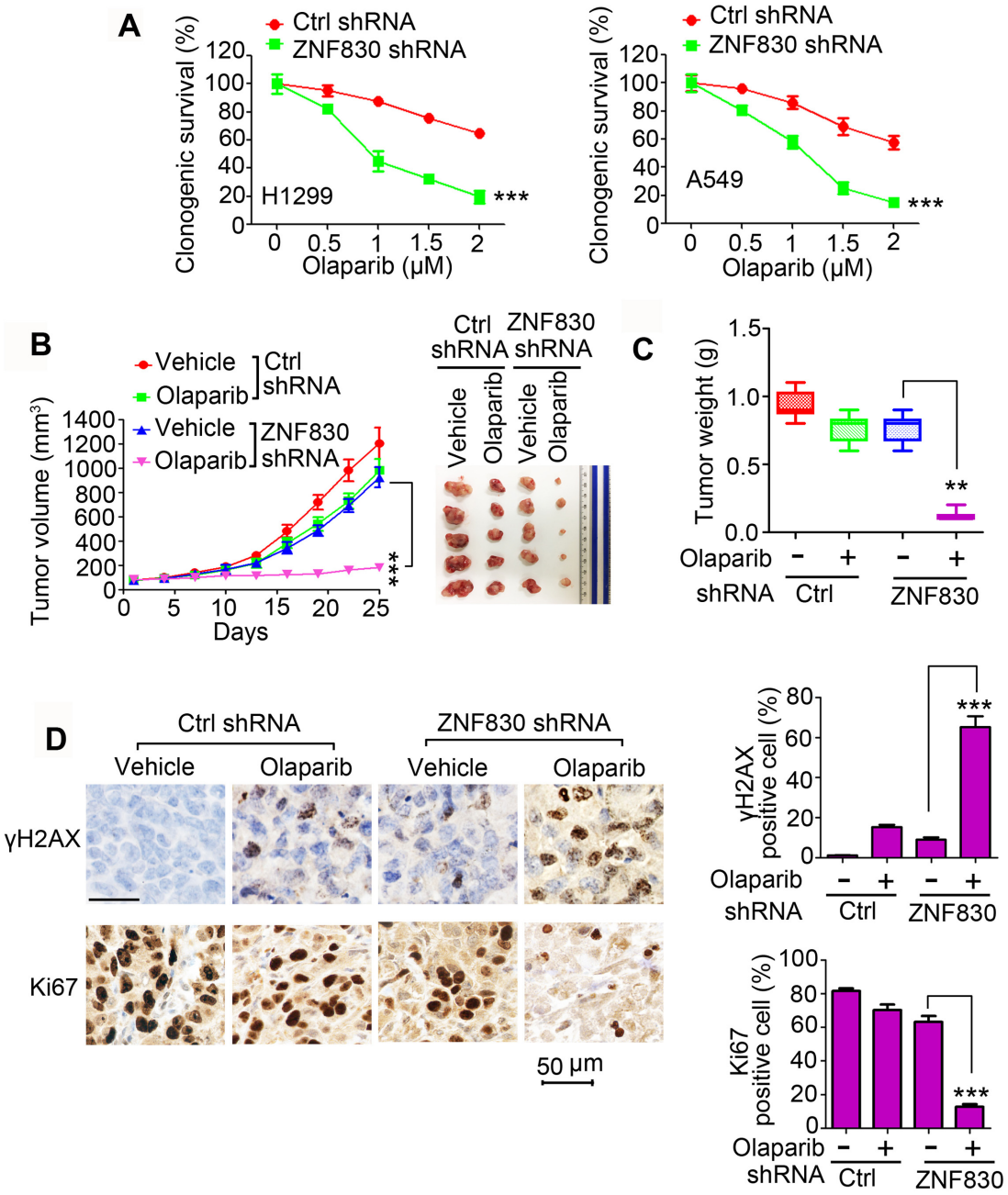

Figure 7. Knock down of ZNF830 sensitize lung cancerxenograft to olaparib. (**A**) H1299 or A549 cells stable expressing ctrl or ZNF830 shRNA were cultured for 10 days in presence of indicated doses of olaparib, The surviving colonies were counted and the relative colony survivals were normalized to untreated cells. (**B**) Tumor growth of indicated H1299 xenografts treated with vehicle or 50 mg/kg olaparib. Left, tumor growth curve; Right, tumor picture for each group was displayed. (**C**) Tumor weight for indicated treatment. (**D**) IHC staining of γH2AX and Ki67 for the tumors isolated from the indicated treatment. Left, representative image of the staining; Right, percentage of γH2AX and Ki67 positive cells were quantified from three independent samples. $^{**}P < 0.01$; $^{***}P < 0.001$. Data presented as mean ± SD of three independent replicates.

The high reliance on DNA repair pathway to survive chemotherapies and radiotherpies might be the Achilles' heel of cancer cells. Other than olaparib, many small molecule DNA repair inhibitors targeting PARP, MGMT, DNA-PK and ATR are already in the pipeline (46). With the experience of olaparib's success in BRCA1/2-mutated breast cancer patients, the status of HR-mediated DNA repair might also play an important role in determining tumor response to the new DNA repair inhibitors. Similar to BRCA1, loss of ZNF830 also rendered H1299 lung cancer xenografts hypersensitive to olaparib treatment in our study, suggesting that ZNF830 can also be used as a predictive marker for olaparib response. According to the results of domain mapping analysis, ZNF830 binds to CtIP through its coiled coil domain, which is essential for ZNF830 functioningin DNA end resection (Figure 5E, Supplementary Figure S5B). Blocking peptides targeting the interacting surface of ZNF830 and CtIP, as well as siR-

NAs targeting ZNF830 might benefits cancer patients by extending the application of small molecule DNA repair inhibitors such as olaparib to patients without defects in HR-mediated DNA repair.

In summary, our study not only identifies novel functions of nuclear protein ZNF830 in HR-mediated DNA repair, but also provides a rational target for enhancing therapeutic efficacy of chemotherapy by the inhibition of ZNF830, particular for PARP1 inhibitor.

SUPPLEMENTARY DATA

Supplementary Data are available at NAR online.

FUNDING

National Natural Science Foundation of China [81772010 to F.W., 81571721 to F.W., 81571799 to H.W., 81773193 to H.W., 81730108 to T.X., and 81602435 to W.L.]; Natural Science Basis Research Plan in Shanxi Province of China [2016JM8016 to F.W.]; Key Project of Zhejiang Province Ministry of Science and Technology [2015C03055 to T.X.]; Funding for open access charge: National Natural Science Foundation of China.
Conflict of interest statement. None declared.

REFERENCES

1. Ochi,T., Blackford,A.N., Coates,J., Jhujh,S., Mehmood,S., Tamura,N., Travers,J., Wu,Q., Draviam,V.M., Robinson,C.V. *et al.* (2015) DNA repair. PAXX, a paralog of XRCC4 and XLF, interacts with Ku to promote DNA double-strand break repair. *Science*, **347**, 185–188.
2. Fugger,K., Chu,W.K., Haahr,P., Kousholt,A.N., Beck,H., Payne,M.J., Hanada,K., Hickson,I.D. and Sorensen,C.S. (2013) FBH1 co-operates with MUS81 in inducing DNA double-strand breaks and cell death following replication stress. *Nat. Commun.*, **4**, 1423.
3. Jeggo,P.A., Pearl,L.H. and Carr,A.M. (2016) DNA repair, genome stability and cancer: a historical perspective. *Nat. Rev. Cancer*, **16**, 35–42.
4. Shrivastav,M., De Haro,L.P. and Nickoloff,J.A. (2008) Regulation of DNA double-strand break repair pathway choice. *Cell Res.*, **18**, 134–147.
5. Chapman,J.R., Taylor,M.R. and Boulton,S.J. (2012) Playing the end game: DNA double-strand break repair pathway choice. *Mol. Cell*, **47**, 497–510.
6. Escribano-Diaz,C., Orthwein,A., Fradet-Turcotte,A., Xing,M., Young,J.T., Tkac,J., Cook,M.A., Rosebrock,A.P., Munro,M., Canny,M.D. *et al.* (2013) A cell cycle-dependent regulatory circuit composed of 53BP1-RIF1 and BRCA1-CtIP controls DNA repair pathway choice. *Mol. Cell*, **49**, 872–883.
7. Yun,M.H. and Hiom,K. (2009) CtIP-BRCA1 modulates the choice of DNA double-strand-break repair pathway throughout the cell cycle. *Nature*, **459**, 460–463.
8. Gaymes,T.J., North,P.S., Brady,N., Hickson,I.D., Mufti,G.J. and Rassool,F.V. (2002) Increased error-prone non homologous DNA end-joining–a proposed mechanism of chromosomal instability in Bloom's syndrome. *Oncogene*, **21**, 2525–2533.
9. Tadi,S.K., Tellier-Lebegue,C., Nemoz,C., Drevet,P., Audebert,S., Roy,S., Meek,K., Charbonnier,J.B. and Modesti,M. (2016) PAXX Is an accessory c-NHEJ factor that associates with Ku70 and has overlapping functions with XLF. *Cell Rep.*, **17**, 541–555.
10. Broderick,R., Nieminuszczy,J., Baddock,H.T., Deshpande,R., Gileadi,O., Paull,T.T., McHugh,P.J. and Niedzwiedz,W. (2016) EXD2 promotes homologous recombination by facilitating DNA end resection. *Nat. Cell Biol.*, **18**, 271–280.
11. Inano,S., Sato,K., Katsuki,Y., Kobayashi,W., Tanaka,H., Nakajima,K., Nakada,S., Miyoshi,H., Knies,K., Takaori-Kondo,A. *et al.* (2017) RFWD3-mediated ubiquitination promotes timely removal of both RPA and RAD51 from DNA damage sites to facilitate homologous recombination. *Mol. Cell*, **66**, 622–634.
12. Park,J., Long,D.T., Lee,K.Y., Abbas,T., Shibata,E., Negishi,M., Luo,Y., Schimenti,J.C., Gambus,A., Walter,J.C. *et al.* (2013) The MCM8-MCM9 complex promotes RAD51 recruitment at DNA damage sites to facilitate homologous recombination. *Mol. Cell. Biol.*, **33**, 1632–1644.
13. Sartori,A.A., Lukas,C., Coates,J., Mistrik,M., Fu,S., Bartek,J., Baer,R., Lukas,J. and Jackson,S.P. (2007) Human CtIP promotes DNA end resection. *Nature*, **450**, 509–514.
14. Feitelson,M.A., Arzumanyan,A., Kulathinal,R.J., Blain,S.W., Holcombe,R.F., Mahajna,J., Marino,M., Martinez-Chantar,M.L., Nawroth,R., Sanchez-Garcia,I. *et al.* (2015) Sustained proliferation in cancer: Mechanisms and novel therapeutic targets. *Semin. Cancer Biol.*, **35**(Suppl), S25–S54.
15. Cheung-Ong,K., Giaever,G. and Nislow,C. (2013) DNA-damaging agents in cancer chemotherapy: serendipity and chemical biology. *Chem. Biol.*, **20**, 648–659.
16. Nagel,Z.D., Kitange,G.J., Gupta,S.K., Joughin,B.A., Chaim,I.A., Mazzucato,P., Lauffenburger,D.A., Sarkaria,J.N. and Samson,L.D. (2017) DNA repair capacity in multiple pathways predicts chemoresistance in glioblastoma multiforme. *Cancer Res.*, **77**, 198–206.
17. Javle,M. and Curtin,N.J. (2011) The role of PARP in DNA repair and its therapeutic exploitation. *Br. J. Cancer*, **105**, 1114–1122.
18. Matulonis,U.A., Penson,R.T., Domchek,S.M., Kaufman,B., Shapira-Frommer,R., Audeh,M.W., Kaye,S., Molife,L.R., Gelmon,K.A., Robertson,J.D. *et al.* (2016) Olaparib monotherapy in patients with advanced relapsed ovarian cancer and a germline BRCA1/2 mutation: a multistudy analysis of response rates and safety. *Ann. Oncol.*, **27**, 1013–1019.
19. Tutt,A., Robson,M., Garber,J.E., Domchek,S.M., Audeh,M.W., Weitzel,J.N., Friedlander,M., Arun,B., Loman,N., Schmutzler,R.K. *et al.* (2010) Oral poly(ADP-ribose) polymerase inhibitor olaparib in patients with BRCA1 or BRCA2 mutations and advanced breast cancer: a proof-of-concept trial. *Lancet*, **376**, 235–244.
20. Vandormael-Pournin,S., Guigon,C.J., Ishaq,M., Coudouel,N., Ave,P., Huerre,M., Magre,S., Cohen-Tannoudji,J. and Cohen-Tannoudji,M. (2015) Oocyte-specific inactivation of Omcg1 leads to DNA damage and c-Abl/TAp63-dependent oocyte death associated with dramatic remodeling of ovarian somatic cells. *Cell Death Differ.*, **22**, 108–117.
21. Pierce,A.J., Johnson,R.D., Thompson,L.H. and Jasin,M. (1999) XRCC3 promotes homology-directed repair of DNA damage in mammalian cells. *Genes Dev.*, **13**, 2633–2638.
22. Munoz,M.C., Yanez,D.A. and Stark,J.M. (2014) An RNF168 fragment defective for focal accumulation at DNA damage is proficient for inhibition of homologous recombination in BRCA1 deficient cells. *Nucleic Acids Res.*, **42**, 7720–7733.
23. Ismail,I.H., Gagne,J.P., Genois,M.M., Strickfaden,H., McDonald,D., Xu,Z., Poirier,G.G., Masson,J.Y. and Hendzel,M.J. (2015) The RNF138 E3 ligase displaces Ku to promote DNA end resection and regulate DNA repair pathway choice. *Nat. Cell Biol.*, **17**, 1446–1457.
24. Pei,H., Zhang,L., Luo,K., Qin,Y., Chesi,M., Fei,F., Bergsagel,P.L., Wang,L., You,Z. and Lou,Z. (2011) MMSET regulates histone H4K20 methylation and 53BP1 accumulation at DNA damage sites. *Nature*, **470**, 124–128.
25. Liu,W., Zhang,B., Chen,G., Wu,W., Zhou,L., Shi,Y., Zeng,Q., Li,Y., Sun,Y., Deng,X. *et al.* (2017) Targeting miR-21 with sophocarpine inhibits tumor progression and reverses epithelial-mesenchymal transition in head and neck cancer. *Mol. Ther.*, **25**, 2129–2139.
26. Tibbetts,R.S., Brumbaugh,K.M., Williams,J.M., Sarkaria,J.N., Cliby,W.A., Shieh,S.Y., Taya,Y., Prives,C. and Abraham,R.T. (1999) A role for ATR in the DNA damage-induced phosphorylation of p53. *Genes Dev.*, **13**, 152–157.
27. Jonat,W., Maass,H. and Stegner,H.E. (1986) Immunohistochemical measurement of estrogen receptors in breast cancer tissue samples. *Cancer Res.*, **46**, 4296s–4298s.
28. Hart,T., Chandrashekhar,M., Aregger,M., Steinhart,Z., Brown,K.R., MacLeod,G., Mis,M., Zimmermann,M., Fradet-Turcotte,A., Sun,S. *et al.* (2015) High-resolution CRISPR screens reveal fitness genes and genotype-specific cancer liabilities. *Cell*, **163**, 1515–1526.

29. Vancevska,A., Douglass,K.M., Pfeiffer,V., Manley,S. and Lingner,J. (2017) The telomeric DNA damage response occurs in the absence of chromatin decompaction. *Genes Dev.*, **31**, 567–577.
30. Bartek,J. and Lukas,J. (2003) Chk1 and Chk2 kinases in checkpoint control and cancer. *Cancer Cell*, **3**, 421–429.
31. Vriend,L.E., Prakash,R., Chen,C.C., Vanoli,F., Cavallo,F., Zhang,Y., Jasin,M. and Krawczyk,P.M. (2016) Distinct genetic control of homologous recombination repair of Cas9-induced double-strand breaks, nicks and paired nicks. *Nucleic Acids Res.*, **44**, 5204–5217.
32. Falck,J., Coates,J. and Jackson,S.P. (2005) Conserved modes of recruitment of ATM, ATR and DNA-PKcs to sites of DNA damage. *Nature*, **434**, 605–611.
33. Cromie,G.A., Connelly,J.C. and Leach,D.R. (2001) Recombination at double-strand breaks and DNA ends: conserved mechanisms from phage to humans. *Mol. Cell*, **8**, 1163–1174.
34. Chang,H.H., Watanabe,G., Gerodimos,C.A., Ochi,T., Blundell,T.L., Jackson,S.P. and Lieber,M.R. (2016) Different DNA end configurations dictate which NHEJ components are most important for joining efficiency. *J. Biol. Chem.*, **291**, 24377–24389.
35. Tomimatsu,N., Mukherjee,B., Catherine Hardebeck,M., Ilcheva,M., Vanessa Camacho,C., Louise Harris,J., Porteus,M., Llorente,B., Khanna,K.K. and Burma,S. (2014) Phosphorylation of EXO1 by CDKs 1 and 2 regulates DNA end resection and repair pathway choice. *Nat. Commun.*, **5**, 3561.
36. Unno,J., Itaya,A., Taoka,M., Sato,K., Tomida,J., Sakai,W., Sugasawa,K., Ishiai,M., Ikura,T., Isobe,T. *et al.* (2014) FANCD2 binds CtIP and regulates DNA-end resection during DNA interstrand crosslink repair. *Cell Rep.*, **7**, 1039–1047.
37. Moynahan,M.E. and Jasin,M. (2010) Mitotic homologous recombination maintains genomic stability and suppresses tumorigenesis. *Nat. Rev. Mol. Cell Biol.*, **11**, 196–207.
38. Ray Chaudhuri,A., Callen,E., Ding,X., Gogola,E., Duarte,A.A., Lee,J.E., Wong,N., Lafarga,V., Calvo,J.A., Panzarino,N.J. *et al.* (2016) Replication fork stability confers chemoresistance in BRCA-deficient cells. *Nature*, **535**, 382–387.
39. Gong,Y., Handa,N., Kowalczykowski,S.C. and de Lange,T. (2017) PHF11 promotes DSB resection, ATR signaling, and HR. *Genes Dev.*, **31**, 46–58.
40. Shiotani,B. and Zou,L. (2009) Single-stranded DNA orchestrates an ATM-to-ATR switch at DNA breaks. *Mol. Cell*, **33**, 547–558.
41. Murray,R.J., Tanteles,G.A., Mills,J., Perry,A., Peat,I., Osman,A., Chan,S., Cheung,K.L., Chakraborti,P.R., Woodings,P.L. *et al.* (2011) Association between single nucleotide polymorphisms in the DNA repair gene LIG3 and acute adverse skin reactions following radiotherapy. *Radiother. Oncol.*, **99**, 231–234.
42. Chen,Y., Liu,H., Zhang,H., Sun,C., Hu,Z., Tian,Q., Peng,C., Jiang,P., Hua,H., Li,X. *et al.* (2017) And-1 coordinates with CtIP for efficient homologous recombination and DNA damage checkpoint maintenance. *Nucleic Acids Res.*, **45**, 2516–2530.
43. Liu,H., Zhang,H., Wang,X., Tian,Q., Hu,Z., Peng,C., Jiang,P., Wang,T., Guo,W., Chen,Y. *et al.* (2015) The deubiquitylating enzyme USP4 cooperates with CtIP in DNA double-strand break end resection. *Cell Rep.*, **13**, 93–107.
44. Kuraoka,I., Ito,S., Wada,T., Hayashida,M., Lee,L., Saijo,M., Nakatsu,Y., Matsumoto,M., Matsunaga,T., Handa,H. *et al.* (2008) Isolation of XAB2 complex involved in pre-mRNA splicing, transcription, and transcription-coupled repair. *J. Biol. Chem.*, **283**, 940–950.
45. Onyango,D.O., Howard,S.M., Neherin,K., Yanez,D.A. and Stark,J.M. (2016) Tetratricopeptide repeat factor XAB2 mediates the end resection step of homologous recombination. *Nucleic Acids Res.*, **44**, 5702–5716.
46. Martin,S.A., Lord,C.J. and Ashworth,A. (2008) DNA repair deficiency as a therapeutic target in cancer. *Curr. Opin. Genet. Dev.*, **18**, 80–86.